Universidad Carlos III de Madrid
e-Archivo

Institutional Repository
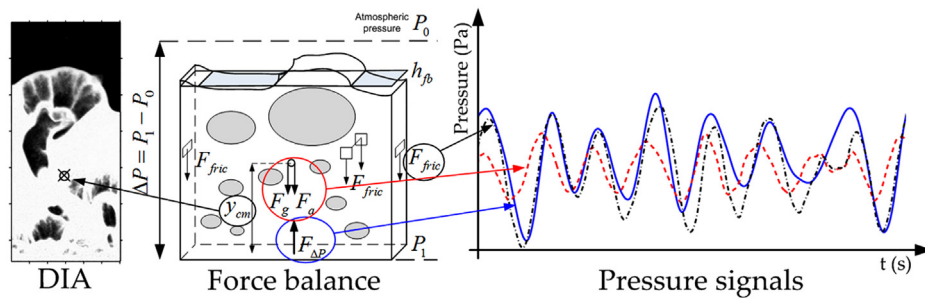
Experimental quantification of the particle–wall frictional forces in pseudo-2D gas fluidised beds

F. Hernández-Jiménez *, J. Sánchez-Prieto, A. Soria-Verdugo, A. Acosta-Iborra *Universidad Carlos III of*

Madrid, Department of Thermal and Fluid Engineering, Av. de la Universidad, 30, 28911, Leganés, Madrid, Spain

GRAPHICAL ABSTRACT

Abstract: In this work a novel measurement technique for pseudo-2D fluidised beds is developed. The objective is to give an estimation of the overall frictional force between the solids and the front and rear walls of the bed. For doing this, the measured pressure signal in the bed is processed in combination with the solids distribution (i.e. centre of mass position, velocity and acceleration) obtained from digital image analysis of the optically accessible front view of the bed. This is performed by acquiring the pressure signal in the bed simultaneously to the digital images. Both the pressure and the digital images are connected through a simple force balance in the bed, and a particle–wall interaction coefficient is obtained assuming that the overall frictional force is proportional to the centre of mass velocity. The particle–wall interaction coefficient found using this technique is of the order of 40–120 kg/m^2 s in the bed tested, and the standard deviation of the frictional forces reaches more than 70% of the weight of the bed. Therefore, the results indicate that the contribution of the particle-to-wall friction on the fluctuation of the pressure drop in a pseudo-2D bed is not negligible.

Keywords: Fluidised bed, Pseudo-2D, Wall effect, Friction, Force balance.

1. Introduction

Fluidised beds have various applications in industry, such as fluid catalytic cracking (FCC), gasification, combustion of solid fuels, and Fischer–Tropsch synthesis (Kunii and Levenspiel, 1991). Despite the fact that fluidised beds have been used in industry since the 1920s and great progress has been made, some aspects of fluidised bed dynamics are still far from being fully understood.

Beds having small thickness, i.e. pseudo two-dimensional (2D) beds, have been crucial for the understanding of the dynamics of gas-particle systems. In this regard, pseudo-2D fluidised bed systems typically have a transparent wall, in order to allow optical access to the system, and possess a small thickness to ensure that the visualisation is representative of the whole system. In this kind of systems, Digital Image Analysis (DIA) or Particle Image Velocimetry

* Corresponding author. Tel.: +34 91 624 6223.
  E-mail address: fhjimene@ing.uc3m.es (F. Hernández-Jiménez).

(PIV) can be applied to characterise the bubble phase and the solids motion, respectively. Such studies have been proved to be a valuable tool for the understanding of fluidised bed systems (Shen et al., 2004; Santana et al., 2005; Almendros-Ibáñez et al., 2006; Müller et al., 2007; Laverman et al., 2008; Busciglio et al., 2008; Sánchez-Delgado et al., 2010; Hernández-Jiménez et al., 2011a,b; Soria-Verdugo et al., 2011a,b; Sánchez-Delgado et al., 2013).

Alternatively, pressure signal analysis is widely used in the literature to characterise the dynamics of fluidised bed systems. Many works have been done in this field and nowadays the pressure signal is routinely employed to obtain a large amount of information concerning the dynamics of a fluidised bed, c.f. the review by van Ommen et al. (2011).

Computational Fluid Dynamics (CFD) can be a very effective complementary tool to the experiments for achieving a detailed analysis of hydrodynamics in complex gas-solids flows. Note that, in these pseudo-2D beds, the front and the rear walls restrict the solids motion, leading to a different flow behaviour compared to fully three- dimensional (3D) systems. For thin bed thicknesses, the effect of the front and the rear wall on the particle motion can be significant and should not be neglected in numerical simulations of pseudo-2D beds (Li et al., 2010; Hernández-Jiménez et al., 2011a). However, there is a lack of experimental quantification of the wall frictional forces in pseudo-2D beds. Knowledge of the wall frictional forces in thin beds can be useful in the understanding of fluidised beds and will facilitate the development of particle–wall interaction models and the validation of the different simulation approaches such as two-fluid models.

The gas pressure field in the bed can be inferred from the solids distribution since these two parameters are inextricably linked in bubbling fluidisation (Davidson and Harrison, 1963; Baskakov et al., 1986; van Ommen et al., 2011). This was verified by Croxford and Gilbertson (2011), who estimated the spatial distribution of the pressure in a pseudo 2-D bubbling bed by numerically solving the Davidson and Harrison (1963) quasi-steady potential flow equations of the gas phase. They used, as an input for the equations, the bubbles size and location experimentally measured with a digital camera. Their simulation successfully reproduced the pressure field when the bubbles over a wide region of the bed were considered.

In the present work, a different approach for the pressure drop prediction in the bed is followed noticing that the dynamics of the bed is also described by its centre of mass. In particular, a novel methodology is proposed for coupling the pressure signal analysis with the digital image acquisition of a fluidised pseudo-2D bed in order to give an estimation of the frictional forces exerted by the front and rear walls on the bed particles. Using a force balance, the frictional force between the bed and the walls is estimated here as a function of the instantaneous pressure drop in the bed, the bed weight, and the velocity and acceleration of the centre of mass of the bed. Additionally, results from a pure 2D simulation, i.e. without incorporating the front and rear walls, have been included to show that in the absence of the front and rear walls the pressure and the acceleration of the centre of mass of the bed are perfectly correlated.

2. Experimental setup

The experimental facility employed in this work is a pseudo-2D cold fluidised bed of dimensions $0.3 \text{ m} \times 1 \text{ m} \times 0.01 \text{ m}$ (width W, height H, and thickness Z). The bed was filled with ballotini glass particles of 2500 kg/m³ density. The experiments were carried out for three different particle sizes: Geldart's classification type B of 0.4–0.6 mm diameter, type B-D particles of 0.6–0.8 mm diameter, and type D particles of 1–1.3 mm diameter. The air distributor

Table 1
Experimental setup.

Parameter		Value
Bed height, H (m)		1
Bed width, W (m)		0.3
Bed thickness, Z (m)		0.01
Aspect ratio, h_0/W (-)		0.75, 1, 1.25
Particles density, ρ_s (kg/m³)		2500
Small particles	d_p (mm)	0.4–0.6
	U_{mf} (m/s)	0.27
Medium particles	d_p (mm)	0.6–0.8
	U_{mf} (m/s)	0.44
Big particles	d_p (mm)	1–1.3
	U_{mf} (m/s)	0.67

consists of a perforated plate with two rows of 30 holes of 1 mm diameter arranged in a triangular configuration with 1 cm pitch. The front and rear walls of the bed were made of glass and the rear wall was painted in black to increase contrast in the front images. A sum up of the experimental parameters is included in Table 1.

A pressure probe was used to carry out the measurements. The probe was placed inside the bed at 5 cm above the distributor plate. The pressure fluctuations in the bed were measured with an ELLISON (PR 3110) differential pressure transducer. The transducer was connected to the probe by means of a silicon tube with a total length of 50 cm and an inner diameter of 4 mm. According to van Ommen et al. (2004) pressure waves in a bubbling bed at $2U_{mf}$ can be detected at radial distances up to 0.3 m from their origin. Also, Croxford et al. (2005) reported that for a small-scale fluidised bed one probe is sufficient, in principle, to characterise the bed hydrodynamics. Therefore, only the pressure probe at 5 cm above the distributor will be used in the bed studied here. In addition, two spotlights were used to get a uniform illumination of the front of the bed. A digital camera, Basler A640, took images of the front view of the fluidised bed at 100 frames per second and, simultaneously, the pressure transducers recorded the pressure signal at 2000 Hz. Fig. 1 shows a scheme of the facility and an example of a greyscale image acquired with the digital camera.

3. Theory

A simple balance of vertical forces in a control volume comprising the gas and particles in a fluidised bed is shown in Fig. 2. The balance indicates that the force exerted by the pressure drop in the bed, ΔP, just over the area $A_T = WZ$ of the distributor, i.e. $F_{\Delta P} = A_T \Delta P$, must compensate to the inertia force due to the acceleration of the centre of mass of the bed, F_a, plus the force due to the weight of the bed, F_g, (i.e. hydrostatic pressure) and the frictional force of the bed walls on the gas and solids phases, F_{fric}:

$$F_{\Delta P} = F_a + F_g + F_{fric} = m\frac{d^2 y_{cm}}{dt^2} + mg + F_{fric} \qquad (1)$$

where $m = A_T(1-\epsilon_0)\rho_s h_0$ is the mass of the bed particles, y_{cm} is the vertical position of the centre of mass of the bed, and $d^2 y_{cm}/dt^2$ is the acceleration of the centre of mass.

In Eq. (1) the inertia and weight of the gas have been neglected since the gas density is much smaller than the particle density. Also, the contribution of the gas phase to the frictional force F_{fric} is expected to be very reduced compared to the frictional force between particles and wall. Note that $F_{\Delta P}$ is equivalent to the force produced by the gas on all the bed particles.

In general, the frictional force is equal to the shear stress, τ, times the surface area of the lateral walls in contact with the bed, $A_L = (2W + 2Z)h_{fb} \approx 2Wh_{fb}$, where h_{fb} is the time-averaged height of the fluidised bed. Following the classical Coulomb's friction
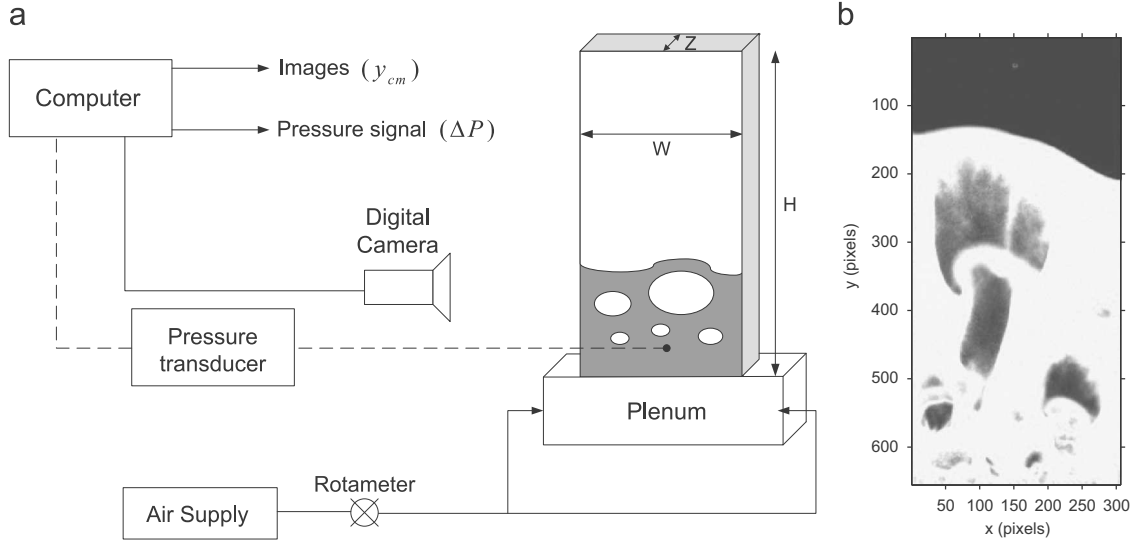
2

Fig. 1. (a) Sketch of the experimental facility and (b) example of a front view image of the fluidised bed.
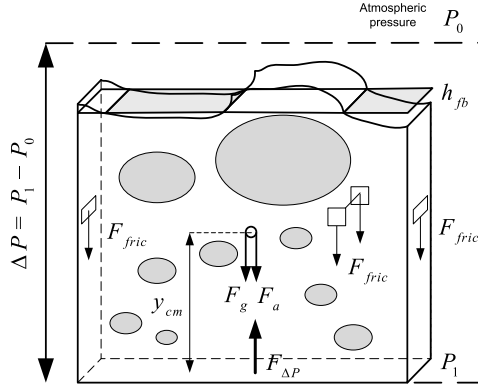

Fig. 2. Balance of forces acting on the bed material. Arrows indicate the direction of the forces when their value is positive in Eq. (1).

model, it will be assumed that the force due to the shear stress is proportional to the normal force times the Coulomb coefficient of friction, $F_{fric} \sim \mu F_N$.

According to the kinetic theory of granular flows, the normal force is a function of the granular temperature of the particles, $F_N \sim f(\Theta)$, and the granular temperature is proportional to the gradient of the particle velocity in perpendicular to the wall $\partial v/\partial n$, (Johnson and Jackson, 1987). The velocity gradient depends on the bed dynamics of the particles in the bed. In the present work, it is postulated that, as a first approximation, the velocity gradient is proportional to the local value of either the velocity of the particles, the acceleration of the particles, or a constant independent of the particle movement. Integrating τ all over the area of the bed walls A_L:

$$F_{fric} = \int_{A_L} \tau \, dA \approx c A_L \Omega \qquad (2)$$

where the frictional form, Ω, can be the instantaneous velocity, dy_{cm}/dt, or the acceleration, $|d^2 y_{cm}/dt^2|\xi$, of the centre of mass of the bed. Frictional forces oppose the direction of the centre of mass velocity, which is mathematically expressed in Ω with $\xi = \text{sign}(dy_{cm}/dy)$. If the frictional force is considered constant (i. e. independent of the bed dynamics), then $\Omega = \xi$. In Eq. (2) c is a proportionality constant that can be interpreted as a new particle–wall interaction coefficient that multiplies $A_L \Omega$ instead of F_N.

The whole balance of forces Eq. (1) can be divided by the transversal area A_T of the bed in order to work with pressures instead of forces:

$$\Delta P = \Delta P_a + \Delta P_g + \Delta P_{fric} = (1 - \epsilon_0)\rho_s h_0 \left(\frac{d^2 y_{cm}}{dt^2} + g \right) + c \frac{A_L}{A_T} \Omega \qquad (3)$$

Note that the term $(1 - \epsilon_0)\rho_s h_0 g$ in Eq. (3) corresponds to the mass of solids in the bed. This term is kept constant in the calculations.

4. Data processing

4.1. Initial processing

Pressure signals and front-view digital images of the pseudo-2D bed were acquired simultaneously, at 2000 Hz and 100 Hz respectively, during $T = 300$ s using the software LabView®. The pressure signal was resampled to 100 Hz to make its temporal resolution equal to the digital images. All the processing described in this section was programmed using the software MATLAB®.

The procedure employed to measure the pressure drop in the bed, ΔP_{meas}, is to use the pressure acquired at $y_P = 5$ cm over the distributor, ΔP_P, and scale it using the averaged weight of the column of particles within this measurement point and the distributor.

$$\Delta P_{meas} \approx \Delta P_P + \rho_s (1 - \epsilon_{mf}) g y_P \qquad (4)$$

In Eq. (4) ϵ_{mf} is employed because the number of bubbles close to the distributor is very reduced and, according to the two fluid theory, the void fraction in the dense phase takes the value for the minimum fluidisation conditions.

DIA was applied to the acquired images of the bed in order to distinguish between bubbles and dense phase. This allowed for the calculation of the vertical position of the centre of mass of the bed, y_{cm}, at each time instant. The centre of mass is calculated with the grey scale images recorded by the camera using the grey level of each pixel. In the bubbles $\alpha_s = 0$, and the grey level pixels of the image is minimum (≈ 0). Also, in the emulsion phase $\alpha_s \approx \alpha_{mf}$ and the grey level of the pixels is close to the maximum (≈ 255). Following Almendros-Ibáñez et al. (2010), a linear relationship between grey levels and solids volume fraction is assumed.

3

Therefore:

$$y_{cm} = \frac{\int \alpha_s y \, dA}{\int \alpha_s \, dA} \approx \frac{\sum_{i=1}^{N} y_i GL_i}{\sum_{i=1}^{N} GL_i} \tag{5}$$

where y is the vertical distance relative to the distributor, i is the pixel number, N is the total number of pixels in the image and GL is the grey level of each pixel in the images.

4.2. Estimation of the particle–wall interaction coefficient

The force balance presented previously can be employed to make an estimation of the particle–wall interaction coefficient c.

The result of applying Eq. (5) at each time instant is a discrete time series of y_{cm} that is numerically differentiated, using second order finite differences, to obtain the time series of the centre of mass velocity, dy_{cm}/dt, and acceleration, d^2y_{cm}/dt^2.

The particle–wall interaction coefficient is obtained by comparing the time evolution of the pressure drop in the bed, ΔP_{meas} (i.e. pressure drop measured), with the right-hand side of Eq. (3) representing the pressure drop calculated only with the vertical position of the centre of mass of the bed, y_{cm}, in Eq. (3). Therefore, the most probable value of c is estimated by performing the following least square minimisation over the total time period of measurement (T):

$$\min_c \left[\int_0^T (\Delta P_{meas} - \Delta P_{calculated})^2 \, dt \right] \tag{6}$$

where $\Delta P_{calculated}$ is expressed according to Eq. (3) as a function of y_{cm} and Ω.

$$\Delta P_{calculated} = (1 - \epsilon_0) \rho_s h_0 \left[\frac{d^2 y_{cm}}{dt^2} + g \right] + c \frac{A_L}{A_T} \Omega \tag{7}$$

The algorithm used to calculate c is described in Fig. 3. The calculus starts with an estimation of c that is used to obtain the pressure drop calculated, $\Delta P_{calculated}$ (Eq. (7)). Despite the images and the pressure were acquired simultaneously, their synchronisation is not initially perfect because of a hardware delay produced by differences in the response time of activation of the pressure and the digital image measurement systems. This hardware delay, $t_d = d\Delta t$, is estimated with the maximum of the cross-correlation of the two signals, ΔP_{meas} and $\Delta P_{calculated}$. The delay, lower than 10 time points, may be different every time the systems are activated so it has to be calculated for each measurement data set. After adjusting the delay between the two signals, the particle–wall interaction coefficient, c, is obtained from Eq. (6, whose integral is computed using a summation extended over all the signal terms.

$$\min_c \left[\sum_{i=1}^{N-d} (\Delta P_{meas,i} - \Delta P_{calculated,i})^2 \Delta t \right] \tag{8}$$

The whole procedure is repeated starting with the obtained value for c until convergence, which requires over 10 iterations.

Besides, a moving average filter was applied to y_{cm} in order to reduce the spurious high frequencies created by the measurement noise that can be amplified during the differentiation of y_{cm}. As the moving average smooths the signals, it must be applied not only to y_{cm} but also to ΔP_{meas} on each calculation. However, the resulting coefficient c is sensitive to the number of points chosen for the moving average filter, N_f. Alternative filtering strategies were studied (e.g. Butterworth filtering, etc.) and the results were still sensitive to other parameters present in the filters. To solve this issue, c is estimated here for a value of N_f not larger than 200 that minimises the error between the signal measured and the signal calculated, $\Delta P_{calculated,i}$.

4.3. Discrepancy factors

The functional form of the frictional force, Ω in Eq. (2), will be chosen on the basis of a discrepancy factor, δ, that accounts for the differences between the pressure measured, ΔP_{meas}, and the pressure calculated, $\Delta P_{calculated}$. Fig. 4 shows an illustration of the pressure measured and calculated, and the distance between a point on one signal and the other signal. Depending on the way the distance is calculated, two ways of defining the discrepancy factor arise. The vertical discrepancy, δ_V, is a function of d_V which considers only the vertical distance between both signals. The total discrepancy, δ_T, is function of d_T which considers the minimum distance between both signals through any possible direction (see Fig. 4).

$$\delta_V = \sqrt{\frac{1}{N-d} \sum_{i=1}^{N-d} \frac{d_{V,i}^2}{\sigma_{\Delta P_{meas}}^2}} \tag{9}$$

$$\delta_T = \sqrt{\frac{1}{N-d} \sum_{i=1}^{N-d} \frac{d_{T,i}^2}{\sigma_{\Delta P_{meas}}^2}} \tag{10}$$

where $\sigma_{\Delta P_{meas}}$ is the standard deviation of ΔP_{meas} and d_V and d_T have been calculated as follows:

$$d_{V,i} = \Delta P_{meas,i} - \Delta P_{calculated,i}$$

$$d_{T,i}^2 = \min_j d_{i,j}^2$$

$$d_{i,j}^2 = (\Delta P_{meas,i} - \Delta P_{calculated,j})^2 + \left(\frac{\sigma_{\Delta P_{meas}}}{\Delta t_c} \right)^2 ((i-j)/f)^2$$

$$\Delta t_c \approx \frac{1}{f_0} = \frac{\pi}{\sqrt{g/h_0}}$$

where f is the acquisition frequency, 100 Hz, f_0 is the characteristic frequency of the bed oscillation as determined by Baskakov et al. (1986), and i, j are data points for ΔP_{meas} and $\Delta P_{calculated}$, respectively, (see Fig. 4).

As mentioned previously, δ_T has two contributions: the vertical and the horizontal discrepancies. The quadratic vertical contribution of the discrepancy is given in Eq. (10) in relative form by dividing it with the square of a characteristic value that ranges the pressure oscillations (i.e. the square of the standard deviation of the pressure oscillations $\sigma_{\Delta P}^2$). The quadratic horizontal contribution of the discrepancy is normalised with the square of period of the oscillation, Δt_c^2, which is the characteristic value that ranges an oscillation along the horizontal axis (i.e. the time). Since Eq. (10) has only $\sigma_{\Delta P}^2$ in the denominator, the scaling factor $(\sigma_{\Delta P}/\Delta t_c)^2$ is multiplying the quadratic horizontal contribution instead of $(1/\Delta t_c)^2$.

Also, it has to be noticed that the estimation of c (Eq. (8)) considers only the vertical displacements, δ_V, otherwise the comparison between ΔP_{meas} and $\Delta P_{calculated}$ in Eq. (8) would be insensitive to the delay between both signals and could not be correctly calculated in the iterative algorithm described in Fig. 3.

5. Results

5.1. Dependence of the frictional forces

The first part of the results focuses on the dependence form of the frictional forces. The aim of this section is to find the best choice for Ω in Eq. (2). Recall that the functional forms of Ω considered are the velocity of the centre of mass, dy_{cm}/dt, the acceleration of the centre of mass, $|d^2y_{cm}/dt^2|\xi$, or the unity, ξ, if the frictional forces are considered to be constant.
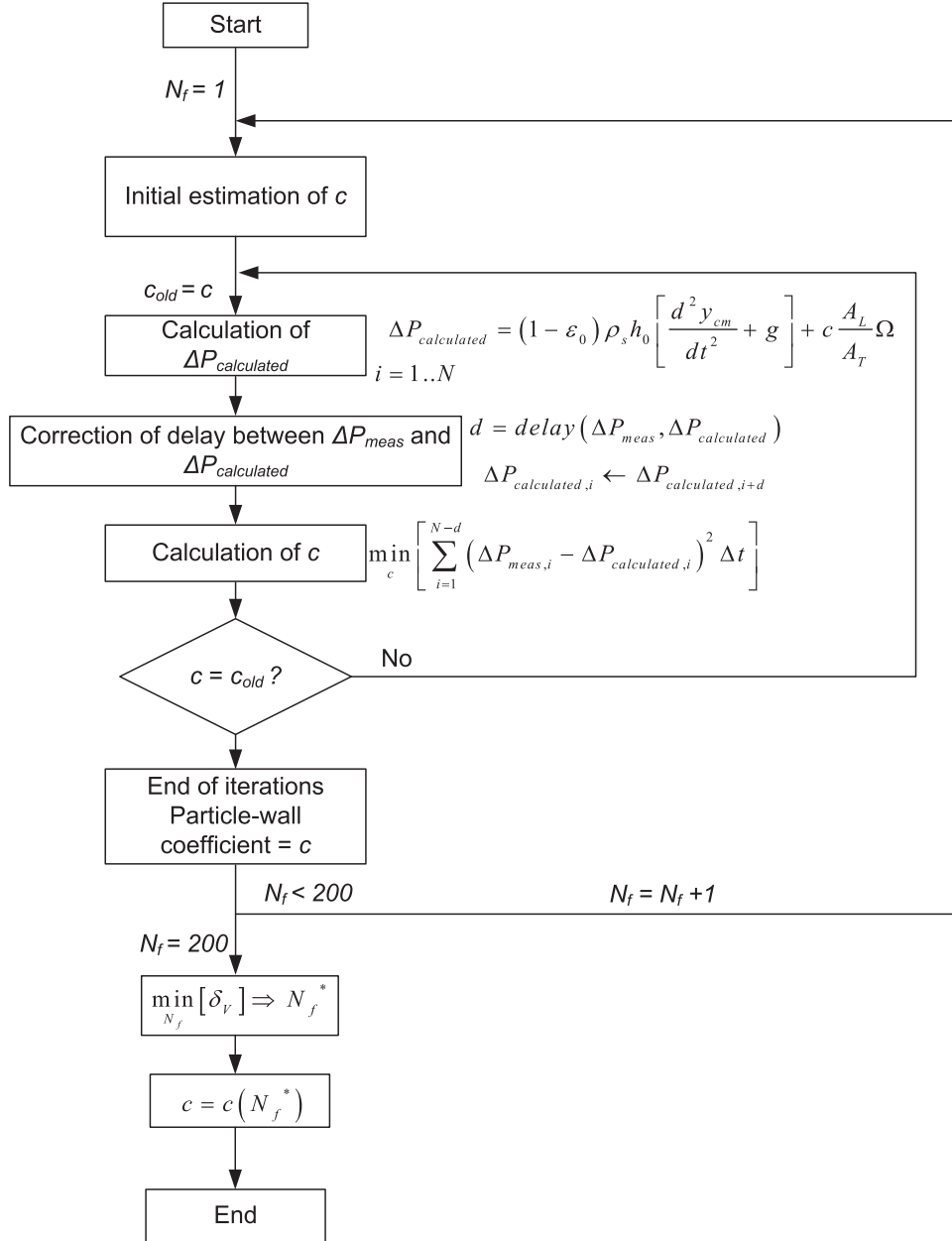
Start

$N_f = 1$

Initial estimation of c

$c_{old} = c$

Calculation of $\Delta P_{calculated}$

$$\Delta P_{calculated} = \left(1 - \varepsilon_0\right)\rho_s h_0 \left[\frac{d^2 y_{cm}}{dt^2} + g\right] + c\frac{A_L}{A_T}\Omega$$

$i = 1..N$

Correction of delay between ΔP_{meas} and $\Delta P_{calculated}$

$d = delay\left(\Delta P_{meas}, \Delta P_{calculated}\right)$

$\Delta P_{calculated,i} \leftarrow \Delta P_{calculated,i+d}$

Calculation of c

$$\min_c \left[\sum_{i=1}^{N-d}\left(\Delta P_{meas,i} - \Delta P_{calculated,i}\right)^2 \Delta t\right]$$

$c = c_{old}$? No

End of iterations Particle-wall coefficient = c

$N_f < 200$ $N_f = N_f + 1$

$N_f = 200$

$$\min_{N_f}\left[\delta_V\right] \Rightarrow N_f^*$$

$$c = c\left(N_f^*\right)$$

End

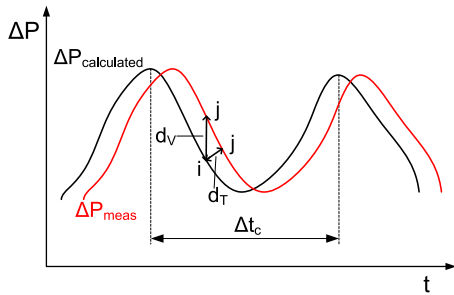Fig. 3. Iterative loop for the calculation of the particle–wall interaction coefficient, c.

Fig. 4. Illustration of the discrepancy factor calculation.

Fig. 5 shows the discrepancy factors, δ_V and δ_T, versus the number of points used in the moving average filter, N_f, for the different choices of the functional form, Ω, and one configuration of the experiments. Analogous results were found for the rest of configurations.

According to Fig. 5, values of δ_V in the range 50–100% are obtained depending on the functional form, Ω. It may seem that the signals ΔP_{meas} and $\Delta P_{calculated}$ are very different since the values found for δ_V are large. However, a small relative displacement of the curves along the horizontal axis (i.e. time in Fig. 4) can substantially increase δ_V even if these signals are identical. To avoid this problem, a better quantification of the discrepancy is the total discrepancy, δ_T, d e fined in Eq. (10), which takes into account the local difference of the signals in both axes of Fig. 4. Using δ_T, the observed discrepancy between ΔP_{meas} and $\Delta P_{calculated}$ is reduced to the range 20–85%.

From Fig. 5 it can be seen that the best functional form of the frictional forces is considering that Ω is proportional to dy_{cm}/dt, since this leads to the smallest discrepancy factor, δ_V and δ_T. Furthermore, the choice of the functional form as a function of the velocity of the particles is in concordance with the fluid-like nature of the dense phase in a fluidised bed. Wall friction forces in a real fluid moving in a parallel-plate channel are proportional

to the bulk velocity of the fluid. When the velocity of the fluid is increased, the velocity gradients are more pronounced and hence the friction forces are higher. Therefore, the force balance that will be considered hereafter is

$$\Delta P = (1-\epsilon_0)\rho_s h_0 \left(\frac{d^2 y_{cm}}{dt^2} + g \right) + c\frac{A_L}{A_T}\frac{dy_{cm}}{dt} \tag{11}$$

Also, a qualitative argument for the choice of Ω proportional to dy_{cm}/dt is presented in Section 5.3 showing the time evolution of the different pressure signals.
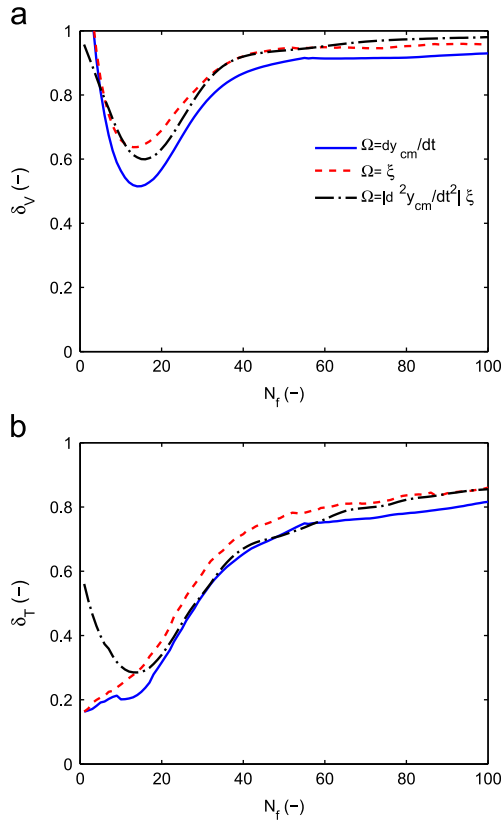
5.2. Simulation evidence

This part shows the results obtained from a two-fluid model 2D simulation of the fluidised bed employed in the experiments. The simulation results are used to check the consistency of the force balance and the algorithms proposed in Section 4. In the simulation, the two-fluid model equations based on the conservation of mass and momentum, together with the balance of granular temperature, were solved using the MFIX code (Multifluid Flow with Interphase eXchanges). The governing equations can be found in Syamlal et al. (1993) and Benyahia et al. (2007).

A second order accurate scheme was selected to discretise the convective derivatives of the governing equations, and the 2D computational domain was meshed using square cells of length 5 mm. The distributor was modelled as a uniform velocity inlet and a fixed pressure boundary condition was chosen at the top of the freeboard. The particle–wall interaction on the lateral walls of the bed was modelled as partial-slip boundary condition, with specularity coefficient equal to 0.6, using the Johnson and Jackson boundary condition for solids (Johnson and Jackson, 1987). The drag model employed for the particle–air interactions was the one proposed by Gidaspow (1994).

The simulation considered particles of 0.5 mm diameter, which corresponds to the average diameter of the particles within the range 0.4–0.6 mm tested in the experiments. The superficial gas velocity was $2U_{mf}$. It has to be noted that the front and rear walls are not presented in the simulation since the numerical domain is 2D, which is equivalent to having front and rear walls with null particle–wall interaction coefficient.

Fig. 6 shows the simulation results concerning (i) the instantaneous pressure of the gas, spatially averaged along the width W, at the bottom of the bed ($\Delta P_{meas,bottom}$), (ii) the pressure calculated ($\Delta P_{calculated}$), and (iii) the pressure measured by a virtual probe at 5 cm above the distributor (ΔP_{meas}). In Fig. 6, the simulated pressure signal obtained at $y=5$ cm above the distributor is extrapolated to $y=0$ using the same procedure as in the experimental results, i.e. Eq. (4). It can be clearly seen that both signals, ΔP_{meas} and $\Delta P_{calculated}$, are almost perfectly correlated. The particle–wall interaction coefficient estimated is negligible due to absence of the front and rear walls, and the fact that c is referred per unit area A_L. The little differences between the pressure curves in Fig. 6 can be attributed to the moving average filter employed to soft the acceleration signal and the small friction produced by the lateral walls of the simulated bed.

The experimental $\Delta P_{meas,bottom}$ is quite difficult to measure due to the local variation of pressure created by the jet effect of the orifices of the distributor. However, as the simulation shows in Fig. 6 the pressure measured at 5 cm above the distributor, ΔP_{meas},
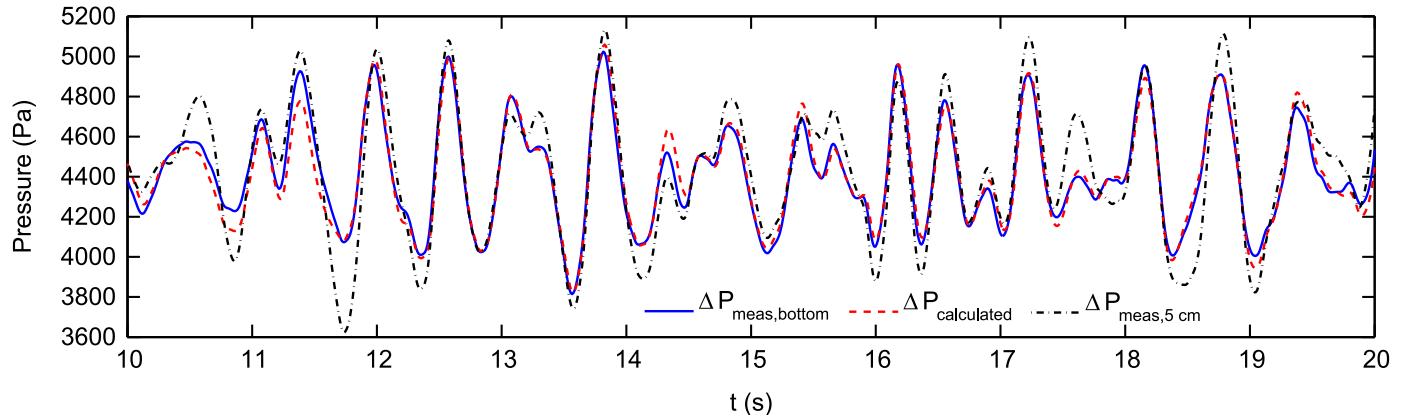

Fig. 5. Discrepancy factor, δ, versus N_f for the different forms of Ω, (a) δ_V, (b) δ_T. Experimental data for $U/U_{mf}=2.5$, $h_0/W=1$ and $d_p=0.4$–0.6 mm.

Fig. 6. Pressure signals at the bottom of the bed ($\Delta P_{meas,bottom}$) and extrapolated from 5 cm above the distributor (ΔP_{meas}), and pressure calculated using the centre of mass of the bed ($\Delta P_{calculated}$). Simulation 2-D results for $U/U_{mf}=2.0$, $h_0/W=1$, $d_p=0.5$ mm, $\Omega=(dy_{cm}/dt)$.

6

also represents fairly well the fluctuations of the pressure at the bottom and can be used as a substitute of $\Delta P_{meas,bottom}$. Discrepancies between $\Delta P_{meas,bottom}$ and ΔP_{meas} are due to the pressure perturbation produced by the passing of small bubbles through the sampling point. Note that in the simulation results the correction of the delay of the signals is not needed since they are perfectly synchronised, and the position of the centre of mass is calculated from the instantaneous snapshots of the void fraction, α_s, instead of the grey level (Eq. (7)).

Therefore, on view of the similitude between ΔP_{meas} and $\Delta P_{calculated}$, the simulation indicates that the force exerted by the pressure drop in the bed is directly linked with the force due to the acceleration of the mass centre of a pure 2D bed (i.e. null front and rear wall frictional forces). The simulations also show that the use of the local pressure measured at 5 cm is a good alternative for estimating the pressure drop in the bed.
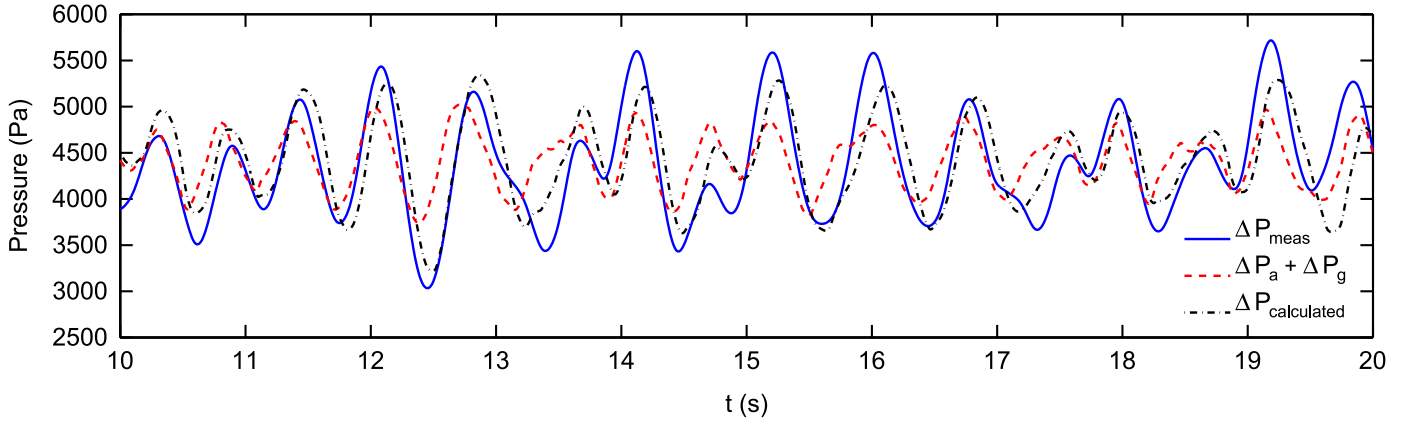
Fig. 7. Pressure signals measured with a probe (ΔP_{meas}), calculated with digital image analysis without considering the frictional forces ($\Delta P_a + \Delta P_g$) and considering them ($\Delta P_{calculated}$). Experimental results for $U/U_{mf} = 2.5$, $h_0/W = 1$, $d_p = 0.4$–0.6 mm, $\Omega = (dy_{cm}/dt)$.
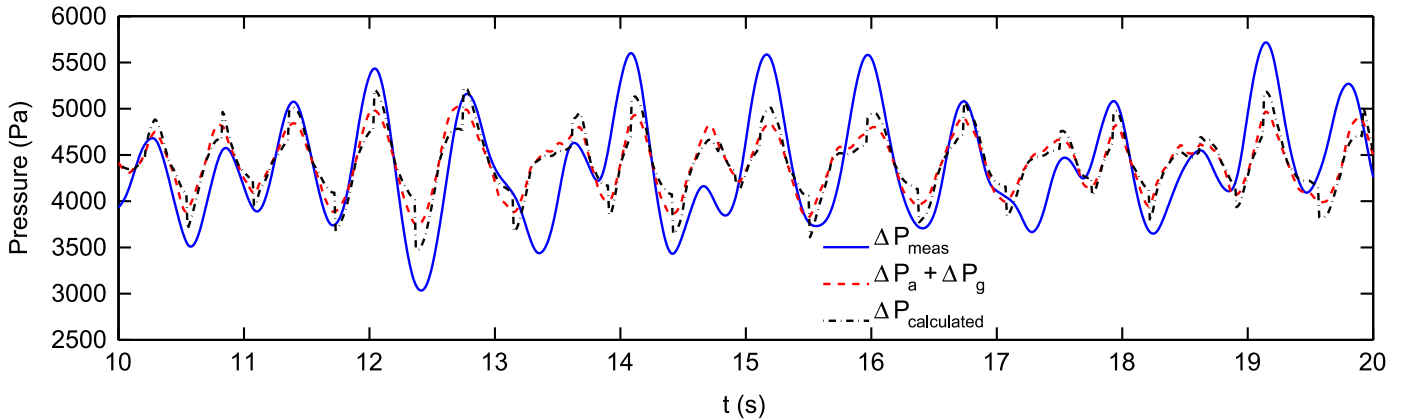
Fig. 8. Pressure signals measured with a probe (ΔP_{meas}), calculated with digital image analysis without considering the frictional forces ($\Delta P_a + \Delta P_g$) and considering them ($\Delta P_{calculated}$). Experimental results for $U/U_{mf} = 2.5$, $h_0/W = 1$, $d_p = 0.4$–0.6 mm, $\Omega = |d^2 y_{cm}/dt^2|\xi$.
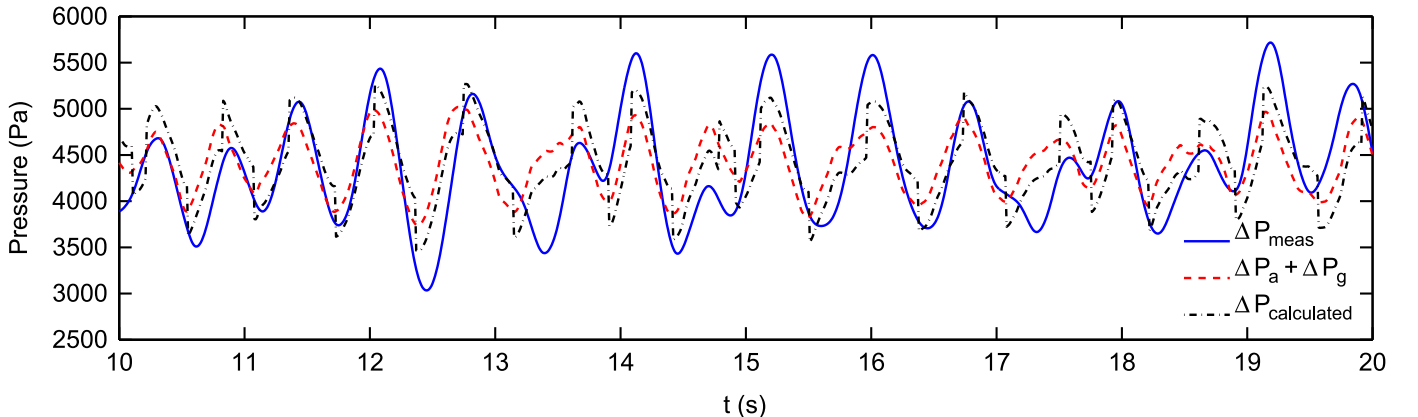
Fig. 9. Pressure signals measured with a probe (ΔP_{meas}), calculated with digital image analysis without considering the frictional forces ($\Delta P_a + \Delta P_g$) and considering them ($\Delta P_{calculated}$). Experimental results for $U/U_{mf} = 2.5$, $h_0/W = 1$, $d_p = 0.4$–0.6 mm, $\Omega = \xi$.

5.3. Experimental quantification of the particle–wall interaction coefficient

Turning now to the experimental results, Fig. 7 shows an illustrative example of the time evolution of the pressure drop measured in the experimental pseudo-2D bed at 5 cm above the distributor (extrapolated using Eq. (4)), ΔP_{meas}, the pressure drop calculated with DIA without considering the frictional forces, $\Delta P_a + \Delta P_g$, and considering them, $\Delta P_{calculated}$. F o r $\Delta P_{calculated}$ the particle–wall interaction coefficient, c, is estimated with the algorithm proposed in Fig. 3. Clearly, the calculation of the pressure drop in the bed with DIA considering the frictional forces is able to reproduce reasonably well most of the oscillations experienced by the pressure measured in the experiment.

Additionally, in Fig. 7 the pressure calculated without considering the frictional forces (c=0) in Eq. (11) is also depicted to illustrate that skipping the frictional forces from the calculation of the pressure produces a wrong prediction of the pressure signal. This shows that the frictional forces are relevant in the force balance in the pseudo-2D bed studied here.

Besides, a qualitative argument for the choice of Ω proportional to dy_{cm}/dt is presented in Figs. 8 and 9, which show the results when considering the functional form proportional to the acceleration of the centre of mass of the bed, or as a constant, respectively. It can be clearly seen that the pressure calculated in these cases cannot reproduce as satisfactorily the oscillations of the pressure measured as the case of $\Omega = dy_{cm}/dt$ (Fig. 7). Furthermore, the calculated signal has an unrealistic and discontinuous behaviour, which can be even worse than the pressure calculated without including the frictional forces.
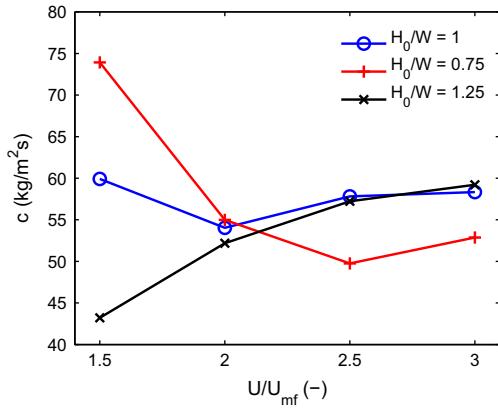

Fig. 10. Experimental particle–wall interaction coefficient, c, versus U/U_{mf} for $d_p = 0.4$–0.6 mm and the three different aspect ratios studied.
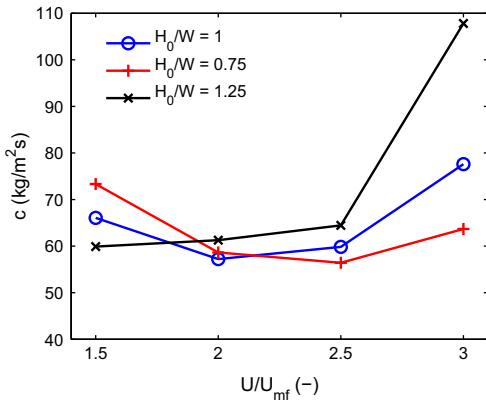

Fig. 11. Experimental particle–wall interaction coefficient, c, versus U/U_{mf} for $d_p = 0.6$–0.8 mm and the three different aspect ratios studied.

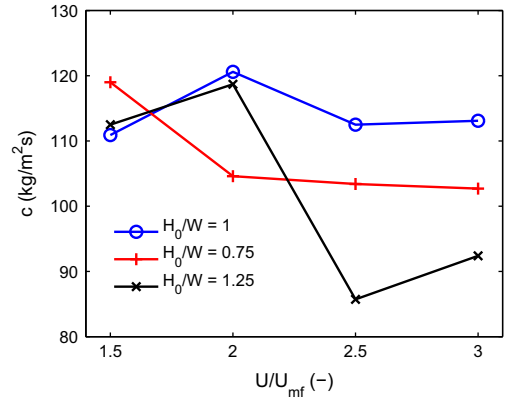**Fig. 12.** Experimental particle–wall interaction coefficient, c, versus U/U_{mf} for $d_p = 1$–1.3 mm and the three different aspect ratios studied.

The particle–wall interaction coefficient, c, can be estimated under the different operative conditions presented in Table 1. For that purpose a set of experiments were done for a range of superficial gas velocities ($U/U_{mf} = 1.5$, 2, 2.5 and 3), static bed aspect ratio ($h_0/W = 0.75$, 1 and 1.25) and particle sizes, $d_p = 0.4$–0.6 mm, 0.6–0.8 mm and 1–1.3 mm. The values of the particle–wall interaction coefficient, c, resulting from these experiments are presented in Figs. 10–12.

Fig. 10 contains the results for the smaller particles ($d_p = 0.4$–0.6 mm) studied in the experiment. It can be seen a small increment of c with the superficial gas velocity for $U > 2U_{mf}$. Also, Fig. 10 shows that the particle–wall interaction coefficient, c, is almost insensitive to the bed aspect ratio. The cases with low velocity ($U = 1.5U_{mf}$) are more disperse and deviate from the latter tendency.

Fig. 11 shows the particle–wall interaction coefficient for the medium size particles ($d_p = 0.6$–0.8 mm). In the medium size particles, the small sensitivity to the aspect ratio is observed again, excepting the results for the high gas velocity ($U = 3U_{mf}$), which may be attributed to a change in the fluidisation regime. Due to the high gas velocity and high fill level, the bubbles in the upper part of the bed cover the whole width of the bed and they produce a regime closer to the slugging operation.

Note that Fig. 11 and, more clearly, Fig. 10 indicate that an increase of the bed aspect ratio produces a growth of the obtained particle–wall interaction coefficient for small superficial gas velocities ($U/U_{mf} = 1.5$). This may be explained considering that the smaller particles tend to create bubbles of small size. As the size of bubbles growths with the distance to the distributor, bubbles are smaller in average in beds of reduced aspect ratio, h_0/W, than in beds of larger h_0/W. Note that the smaller bubbles are more difficult to capture with the DIA because of the rain of particles inside the bubbles. The missing of bubbles reduces the apparent fluctuation of the centre of mass of the bed, which has to be compensated by slightly greater values of c in order to fulfil the force balance used in the method.

To provide an indication of the error associated with the values of c in the figures, the standard deviation of c can be estimated. To do that, the signal recorded can be split in five different signals of 60 s each one to check the repeatability of the measurements. The value obtained for the most unfavourable case (small particles, $1.5U_{mf}$, $H_0/W = 0.75$) was 12.3 kg/m^{2}s. Besides, an indirect indicator of the total error (random plus bias error) in the estimation of the coefficient c is given by the value obtained for the total discrepancy, δ_T, (see for example Fig. 5b), which is around 20% for all the experiments performed. These error estimations can be considered acceptable due to the complexity of the experimental data processing.

The particle–wall interaction coefficient estimated for the biggest particle size studied in the experiments ($d_p = 1$–1.3 mm)
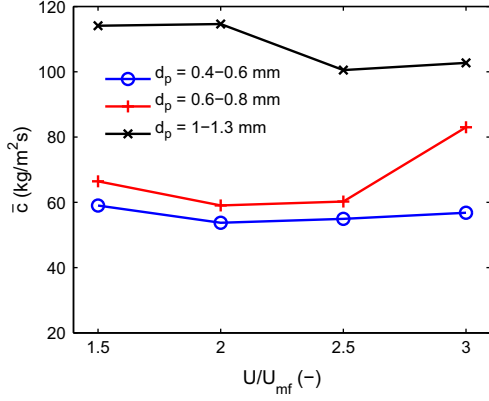
Fig. 13. Comparison of the experimental mean particle–wall interaction coefficient, $\overline{c}$, versus U/U_{mf} for the different particle sizes studied.
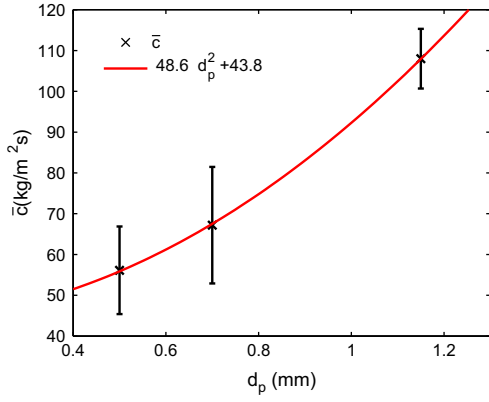
Fig. 14. Experimental mean particle–wall interaction coefficient, $\overline{c}$, versus d_p and fitting curve. The vertical bars denote the standard deviation of the experimental data from the mean.

Fig. 15. Normalised standard deviation of the pressure terms versus U/U_{mf}. Experimental data for $h_0/W = 1$, $d_p = 0.6$–0.8 mm.

is shown in Fig. 12. As for the previous particles, the results for the biggest particles are relatively insensitive to the bed aspect ratio and limitedly sensitive to the superficial gas velocity. Nevertheless, the case for the higher aspect ratio seems to slightly deviate from the tendency of the other two aspect ratios tested.

The previous results suggest that the particle–wall interaction coefficient, c, is weakly affected by the aspect ratio of the bed. Exception of this is, perhaps, the data dispersion observed at low or high superficial velocities. Therefore a robust estimation of the particle–wall interaction coefficient can be made by averaging the particle–wall interaction coefficient obtained for the three aspect ratios, keeping constant U/U_{mf} and d_p. Fig. 13 shows the results of this mean particle–wall interaction coefficient, $\overline{c}$.

In general, the particle–wall interaction coefficient, $\overline{c}$, for the particles of $d_p = 1$–1.3 mm is almost the double than for the other particles. The medium size particles ($d_p = 0.6$–0.8 mm) give values of the mean particle–wall interaction coefficient slightly higher than for the small particles ($d_p = 0.4$–0.6 mm).

Therefore, the experiments indicate that the particle–wall interaction coefficient defined as Eq. (2), with $\Omega = dy_{cm}/dt$, increases substantially with the particle size. The growth of the particle–wall interaction coefficient with the size of the particles may be attributed to the enhancement of the wall effects produced when the number of particles that can be allocated along the transversal direction, Z, of the bed is reduced. In contrast, the variation of $\overline{c}$ with the superficial gas velocity in Fig. 13 is comparatively small and without a defined trend.

Considering that the mean particle–wall interaction coefficient, $\overline{c}$, in Fig. 13 is relatively insensitive to both the aspect ratio and the
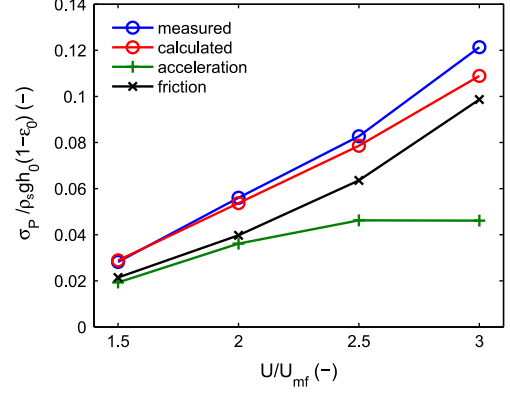
superficial gas velocity, a simple dependence in terms of the particle diameter can be retained, i.e. $\overline{c} = f(d_p)$, in this first experimental characterisation of the value of $\overline{c}$. Fig. 14 plots the mean particle–wall interaction coefficient versus the particle diameter, which is used to fit a function that models $\overline{c}$ versus d_p. In view of Fig. 14 it seems that $\overline{c}$ does not depend linearly on d_p but rather quadratically. Thus, based on the trend found for the present results, a second order polynomial of the form $a_2 d_p^2 + a_1 d_p + a_0$, is selected as a simple example of model function.

According to the constitutive relations for granular materials by Johnson and Jackson (1987), the particle–wall frictional force is not a strong function of the particle diameter. These authors developed their theory considering that the particles were immersed in a very large volume compared to the particle size and that the walls are not close to each other. For the pseudo-2D fluidised bed studied here, the frictional forces clearly depend on the particle diameter. This can be explained considering that in the pseudo-2D bed the volume is not very large since the thickness is in the order of 10 times d_p. Making d_p much smaller than Z, the bed thickness will be seen by a particle as infinitely large. Thus, in order to make the quadratic function model more consistent with the Johnson and Jackson friction constitutive relations, the derivative of $\overline{c}$ with regard d_p must vanish when d_p/Z tends to zero (i.e. $2a_2 d_p + a_1 \rightarrow 0$ when $d_p \rightarrow 0$). This implies that the coefficient $a_1 = 0$ and the polynomial to be fitted is $a_2 d_p^2 + a_0$. The result of the least square regression of this quadratic function to the frictional force data in Fig. 14 is

$$\overline{c} = 48.6(d_p[\text{mm}])^2 + 43.8 \tag{12}$$

Note that in Eq. (12), the particle diameter, d_p, must be introduced in mm.

It has to be said that the results presented here were performed for a pseudo-2D bed of fixed thickness of 1 cm, which means that the proposed correlation may be valid only for beds of such thickness. The root mean square difference between Eq. (12) and all of the individual experimental data in Figs. 10–12 gives a regression error of Eq. (12) equal to 10.7 kg/m²s, which is a 19% of $\overline{c}$ in the most unfavourable case (smallest value of $\overline{\epsilon}$), and 9% in the most favourable case, with an average value of 14%.

The last part of this section focuses on the quantification of the frictional forces relative to the other forces in the bed. Fig. 15 compares the standard deviation of the pressure signals in the bed, $\Delta P_{calculated}$, ΔP_a and ΔP_{fric}, normalised with the mean pressure drop in the bed due to its weight, $\rho_s g h_0 (1 - \epsilon_0)$. The results correspond to the medium size particles and aspect ratio equal to unity. Similar trends were found for the other particles and aspect ratios. As expected, the measured and the calculated standard deviation of the pressure signal depend linearly on the superficial gas velocity as a result of the growth the bubbles that produce the pressure fluctuations of the bed. Also, Fig. 15

shows that the frictional force is not negligible in the force balance, increasing its relative contribution when the gas velocity is augmented. The frictional forces reach more than the 70% of the force produced by the weight of the bed. The standard deviation of the frictional forces is always superior to the standard deviation of the internal forces. This important result indicates that the impact of the frictional force in the pressure drop oscillations in a pseudo-2D bed is even greater than the contribution of the force produced by the acceleration of the centre of mass at high superficial gas velocities.

6. Conclusions

In this work, the frictional forces exerted by the front and rear walls on the solids of a pseudo-2D fluidised bed were experimentally characterised. This was done by linking the pressure drop measured in the bed with the acceleration and velocity of its centre of mass obtained from digital image measurements of the solids distribution. The frictional forces were assumed to be a function of the bed dynamics and it was found that the best choice is to consider the friction proportional to the solids velocity through a particle–wall interaction coefficient, c. The resulting coefficient was in the range of 40–120 kg/m^{2}s for the operative conditions studied in the present work. In general the particle–wall interaction coefficient, c, was found to be very sensitive to the particle diameter, less affected by the superficial gas velocity and weakly affected by the bed aspect ratio. The fluctuations of the frictional forces on the pressure drop in the bed resulted to be even larger than the fluctuations induced by the acceleration of the bulk of the bed. These empirical findings evidence that the friction of particles with the walls plays an important role in the dynamics of pseudo-2D beds.

Nomenclature

A_L	lateral area (m^2)
A_T	transversal area (m^2)
c	particle–wall interaction coefficient (kg/m^{2}s)
d	delay points (-)
d_p	particle diameter (mm)
f	acquisition frequency (Hz)
f_0	characteristic pressure frequency (Hz)
$F_{\Delta P}$	force due to the pressure drop in the bed (N)
F_a	force due to the acceleration of the centre of mass of the bed (N)
F_g	force due to the bed weight (N)
F_{fric}	frictional forces (N)
F_N	normal force (N)
GL	grey level of the pixels (-)
g	gravity (m/s^2)
H	bed height (m)
h_{fb}	mean freeboard height (m)
h_0	static bed height (m)
m	mass of the bed (kg)
N	number of pixels (-)
N_f	number of points of the moving average filter (-)
n	normal direction to the wall (-)
ΔP	pressure drop in the bed (Pa)
ΔP_{meas}	pressure drop measured (Pa)
$\Delta P_{calculated}$	pressure drop calculated (Pa)
ΔP_p	pressure drop at 5 cm over the distributor (Pa)
T	total measurement time (s)
t_d	time delay (s)
Δt	sampling time interval (s)
U	superficial gas velocity (m/s)

U_{mf}	minimum fluidisation velocity (m/s)
v	solids velocity (m/s)
y_{cm}	vertical position of the centre of mass of the bed (m)
y_p	vertical position of the pressure probe (cm)
W	bed width (m)
Z	bed thickness (m)

Greek letters

α_s	solids volume fraction (-)
α_{mf}	solids volume fraction at minimum fluidisation conditions (-)
δ	discrepancy factor (-)
δ_v	vertical discrepancy factor(-)
δ_T	total discrepancy factor (-)
ϵ_0	static bed void fraction (-)
ϵ_{mf}	bed void fraction at minimum fluidisation conditions (-)
μ	Coulomb coefficient of friction (-)
Ω	functional of the frictional force (-)
ρ_s	solids density (kg/m^3)
τ	shear stress (N/m^2)
θ	granular temperature (J/kg)
$\sigma_{\Delta P}$	standard deviation of the pressure (Pa)
ξ	direction of the centre of mass velocity

References

Almendros-Ibáñez, J.A., Sobrino, C., de Vega, M., Santana, D., 2006. A new model for ejected particle velocity from erupting bubbles in 2-D fluidized beds. Chemical Engineering Science 61, 5981–5990.

Almendros-Ibáñez, J.A., Pallarès, D., Johnsson, F., Santana, D., 2010. Voidage distribution around bubbles in a fluidized bed: influence on throughflow. Powder Technology 197, 73–82.

Baskakov, A.P., Tuponogov, V.G., Filippovski, N.F., 1986. A study of pressure fluctuations in a bubbling fluidized bed. Powder Technology 45, 113–117.

Benyahia, S., Syamlal, M., O'Brien, T.J., 2007. Summary of MFIX equations 2005-4.

Busciglio, A., Vella, G., Micale, G., Rizzuti, L., 2008. Analysis of the bubbling behaviour of 2D gas solid fluidized beds: part I. Digital image analysis technique. Chemical Engineering Journal 140, 398–413.

Croxford, A.J., Harrison, A.J.L., Gilbertson, M.A., 2005. The optimisation of pressure measurements for the control of bubbling fluidised beds. International Journal of Chemical Reactor Engineering 3, A39.

Croxford, A.J., Gilbertson, M.A., 2011. Pressure fluctuations in bubbling gas-fluidized beds. Chemical Engineering Science 16, 3569–3578.

Davidson, J.F., Harrison, D., 1963. Fluidised Particles. Cambridge University Press, Cambridge.

Gidaspow, D., 1994. Multiphase Flow and Fluidization: Continuum and Kinetic Theory Descriptions. Academic Press, San Diego, CA.

Hernández-Jiménez, F., Sánchez-Delgado, S., Gómez-García, A., Acosta-Iborra, A., 2011a. Comparison between two-fluid model simulations and particle image analysis & velocimetry (PIV) results for a two-dimensional gas-solid fluidized bed. Chemical Engineering Science 66, 3753–3772.

Hernández-Jiménez, F., Third, J.R., Acosta-Iborra, A., Müller, C.R., 2011b. Comparison of bubble eruption models with two-fluid simulations in a 2D gas-fluidized bed. Chemical Engineering Journal 171, 328–339.

Johnson, P.C., Jackson, R., 1987. Frictional collisional constitutive relations for granular materials, with application to plane shearing. Journal of Fluid Mechanics 176, 6793.

Kunii, D., Levenspiel, O., 1991. Fluidization Engineering. Butterworth-Heinemann, Newton, MA.

Laverman, J.A., Roghair, I., van Sint Annaland, M., Kuipers, H., 2008. Investigation into the hydrodynamics of gas-solid fluidized beds using particle image velocimetry coupled with digital image analysis. Canadian Journal of Chemical Engineering 86, 523–535.

Li, T., Grace, J.R., Bi, X., 2010. Study of wall boundary condition in numerical simulations of bubbling fluidized beds. Powder Technology 203, 447–457. Müller, C.R., Davidson, J.F., Dennis, J.S., Hayhurst, A.N., 2007. A study of the motion and eruption of a bubble at the surface of a two-dimensional fluidized bed using particle image velocimetry (PIV). Industrial & Engineering Chemistry Research 46, 1642–1652.

Sánchez-Delgado, S., Marugán-Cruz, C., Acosta-Iborra, A., Santana, D., 2010. Dense-phase velocity flu c t u a t i o n i n a 2 - D fluidized bed. Powder Technology 200, 37–45.

Sánchez-Delgado, S., Marugán-Cruz, C., Soria-Verdugo, A., Santana, D., 2013. Estimation and experimental validation of the circulation time in a 2D gas-solid fluidized beds. Powder Technology 235, 669–676.

Santana, D., Nauri, S., Acosta, A., Garcia, N., Macias-Machin, A., 2005. Initial particle velocity spatial distribution from 2-D erupting bubbles in fluidized bed. Powder Technology 150, 1–8.

Shen, L., Johnsson, F., Leckner, B., 2004. Digital image analysis of hydrodynamics two-dimensional bubbling fluidized beds. Chemical Engineering Science 59, 2607–2617.

Soria-Verdugo, A., García-Gutíerrez, L.M., Sánchez-Delgado, S., Ruiz-Rivas, U., 2011a. Circulation of an object immersed in a bubbling fluidized bed. Chemical Engineering Science 66, 78–87.

Soria-Verdugo, A., García-Gutiérrez, L.M., García-Hernando, N., Ruiz-Rivas, U., 2011b. Buoyancy effects on objects moving in a bubbling fluidized bed. Chemical Engineering Science 66, 2833–2841.

Syamlal, M., Rogers, W., O'Brien, T.J., 1993. MFIX Documentation: Theory Guide. U.S. Department of Energy (DOE). Morgantown Energy Technology Center, Morgan-town, West Virginia.

van Ommen, van der Schaaf, J., Schouten, J.C., vanWachem, B.G.M., Coppens, M.O., vanderBleek, C.M., 2004. Optimal placement of probes for dynamic pressure measurements in large-scale fluidized beds. Powder Technology 139, 264–276.

van Ommen, R.J., Sasic, S., van der Schaaf, J., Gheorghiu, S., Johnsson, F., Coppens, M. O., 2011. Time-series analysis of pressure fluctuations in gas-solid fluidized beds – a review. International Journal of Multiphase Flow 37, 403–428.